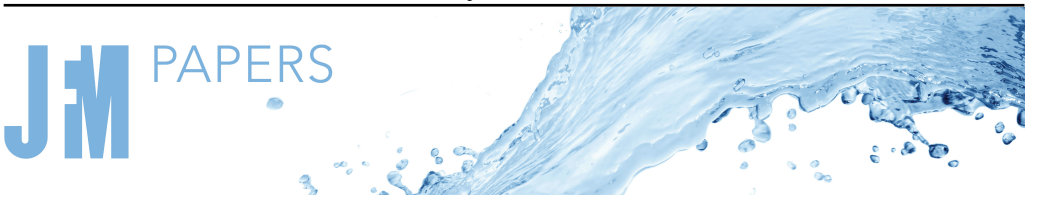
J. Fluid Mech. (2026), *vol.* 1029, A50, doi:10.1017/jfm.2026.11144



Merging of three aligned vortices

Morten Andersen[1], **Peter A. Knudsen**[1], **Marc John Bordier Dam**[1] and **Jesper Schmidt Hansen**[1]

[1]IMFUFA, Department of Science and Environment, Roskilde University, Universitetsvej 1, Roskilde 4000, Denmark

Corresponding author: Morten Andersen, moan@ruc.dk

(Received 1 April 2025; revised 28 October 2025; accepted 21 December 2025)

We investigate two-dimensional vortex merging of three vortices, initially aligned and evenly spaced, with the two outer vortices having the same strength and the middle one having any strength. Based on the vorticity transport equation (VTE) a vortex is identified as an extremum of the vorticity. The vorticity is also investigated through the low-dimensional core-growth model, providing analytical insight into the vorticity patterns and transitions, including explicit formulas of trajectories of the critical points of vorticity. Four distinct vorticity patterns and four types of trajectories of the vorticity are found. For a corotating centre vortex there are two types of trajectories of the vorticity, one where the centre vortex dominates the two outer vortices, and one where the centre vortex is suppressed by the two outer vortices. The two types of trajectories are separated in parameter space by the strength ratio of the inner to outer vortex being $4\exp(-3/2)$. In the case of a counter-rotating vortex centre, the centre vortex is suppressed in the flow transitions for centre vortex strengths less than the sum of the two outer vortices. For a range of vortex strengths of the middle vortex, the three vortex configuration first rotates in one direction and then shifts direction of rotation. In the case of a centre vortex strength exceeding the sum of the two outer vortices, the two outer vortices are pushed away. The core-growth model quantitatively reproduces the VTE flow for low Reynolds number (Re) and topologically provides accurate descriptions up to $Re = 1290$ where filamentation vortices are created.

Key words: bifurcation, low-dimensional models, vortex dynamics

1. Introduction

Vortex dynamics, interaction and merging are fundamental aspects of fluid motion. The dynamics of two vortices has been of great interest and subject to much study both

© The Author(s), 2026. Published by Cambridge University Press. This is an Open Access article, distributed under the terms of the Creative Commons Attribution licence (https://creativecommons.org/licenses/by/4.0/), which permits unrestricted re-use, distribution and reproduction, provided the original article is properly cited.

https://doi.org/10.1017/jfm.2026.11144 Published online by Cambridge University Press

theoretically and experimentally; see Widnall (1975) and Leweke, Dizes & Williamson (2016) for reviews. The merging of three or more vortices has not been studied in similar detail although it is of great interest in order to understand more complex fluid motion emerging in nature or industry. One reason for the lack of study is the increasing complexity, well known in the celestial counterpart – the three body problem. As a step towards understanding the fluid motion of three vortices we here choose a special initial condition for the vortices, although several parameters still have arbitrary values. We investigate theoretically and computationally two-dimensional vortex merging starting with three aligned vortices, as shown in figure 1. In a point vortex setting (i.e. negligible viscosity), this initial configuration is a relative equilibrium, meaning that, depending on the vortex strengths, the vortices will stay fixed or rotate steadily but always maintain their mutual distances. However, in viscous flow, merging will always happen if the sum of the vortex strengths is non-zero since the long-term solution converges to the flow of a single Lamb–Oseen vortex, as proved by Gallay & Wayne (2005). We investigate the viscous merging of three aligned vortices for any centre vortex strength. A special case of this set-up has been investigated by Jing, Kanso & Newton (2010) with the middle vortex rotating oppositely to the outer vortices and with half their strength. The vortex tripole experiment by van Heijst & Kloosterziel (1989) has also been modelled with three aligned vortices and corresponds to the case where the total vorticity vanishes. For small values of the centre vortex, the configuration is a perturbation to the well-studied case of two symmetric vortices (Cerretelli & Williamson 2003; Meunier, Le Dizes & Leweke 2005). A benefit of the set-up chosen here will turn out to be the analytical insight from the core-growth model (described below), owing to the symmetry in the initial condition.

The flow is governed by the vorticity transport equation (VTE) in the unbounded plane

$$\frac{\partial \omega}{\partial t} = -\boldsymbol{u} \cdot \boldsymbol{\nabla} \omega + \nu \Delta \omega, \tag{1.1}$$

where ν is the kinematic viscosity, $\boldsymbol{u}$ is the two-dimensional velocity field and ω is the non-trivial component of the vorticity, defined as the curl of the velocity.

To characterise the flow patterns the vorticity contours are investigated. These are organised by the critical points of the vorticity, $\partial_x \omega(x, y) = \partial_y \omega(x, y) = 0$ which come in two generic variants: local extremal points or saddle points which can be categorised from higher-order derivatives of the vorticity. Extremal points can be identified as vortices in the flow, while the saddle points have no physical interpretation, but must be identified to precisely describe the vortex patterns and their transitions. This approach has previously been used to investigate the occurrence of the von Kármán vortex street (Heil *et al.* 2017) and merging of two vortices (Brøns *et al.* 2025). A similar topological investigation focusing on the streamfunction rather than the vorticity has been used extensively to study other flow configurations (Tobak & Peake 1982; Brøns 2007). The vorticity topology is Galilean invariant, but the streamline topology is not, so we focus on the former here.

We investigate the vorticity contours based on the VTE, and compare the results with the core-growth model which allows for analytical investigation of viscous vortex interaction and merging (Jing, Kanso & Newton 2012; Kim & Sohn 2012). Conveniently expressed in complex form with $z = x + \mathrm{i}y$, the motion of a Gaussian vortex centre at z_j with strength Γ_j is governed by the position of the remaining $N - 1$ vortices

$$\frac{\mathrm{d}\overline{z_j}}{\mathrm{d}t} = \sum_{k \neq j}^{N} \frac{\Gamma_k}{2\pi \mathrm{i}} \frac{1}{z_j - z_k} \left(1 - \exp\left(-\frac{|z_j - z_k|^2}{4\nu t}\right)\right), \tag{1.2}$$

https://doi.org/10.1017/jfm.2026.11144 Published online by Cambridge University Press

where $\overline{z}$ is the complex conjugate of z. The resulting velocity field is

$$\frac{\mathrm{d}\overline{z}}{\mathrm{d}t} = \sum_{k=1}^{N} \frac{\Gamma_k}{2\pi \mathrm{i}} \frac{1}{z - z_k} \left(1 - \exp\left(-\frac{|z - z_k|^2}{4\nu t}\right)\right). \tag{1.3}$$

The corresponding vorticity being the curl of the velocity is

$$\omega(z, t) = \sum_{k=1}^{N} \frac{\Gamma_k}{4\pi \nu t} \exp\left(-\frac{|z - z_k|^2}{4\nu t}\right). \tag{1.4}$$

In our study, $N = 3$ and the initial condition is three point vortices on a straight line, see figure 1,

$$\omega(z, 0) = \Gamma\delta(z - r_0) + \alpha\Gamma\delta(z) + \Gamma\delta(z + r_0). \tag{1.5}$$

The strength of the outer vortices is Γ and the strength of the centre vortex is $\alpha\Gamma$, where $\alpha \in \mathbb{R}$. The case $\alpha = -2$ corresponds to the vortex tripole experiment (van Heijst & Kloosterziel 1989) and the case $\alpha = -0.5$ corresponds to the point vortex equilibrium, studied by Jing *et al.* (2010) with the purpose of elucidating the advection of passive tracers in a flow. For $\alpha = 0$ we retrieve the well-studied case of two corotating vortices (Leweke *et al.* 2016; Andersen *et al.* 2018). The velocity and vorticity given by the core-growth model, (1.2)–(1.4), is only an exact solution to VTE for $N = 1$. However, the core-growth model has shown to be useful to study vortex interaction for $N > 1$ (Kim & Sohn 2012; Nielsen *et al.* 2021; Dam, Hansen & Andersen 2023). Kim & Sohn (2012) show that the core-growth model with N vortices has integrals similar to the well-studied point vortex model, and prove that the well-known possibility of collapse of three point vortices (Synge 1949; Aref 1979) is not possible in the core-growth model. Nielsen *et al.* (2021) use the core-growth model and the Q-criterion to study merging of two vortices. Dam *et al.* (2023) obtain analytical insight into the merging of three vortices initially located at the corners of an equilateral triangle by use of the core-growth model.

We aim to characterise vorticity contours of the core-growth model which requires the following approach: fix values for the parameters ν, Γ, α, r_0 and let the Gaussian vortex centres, z_j, be governed by (1.2) with initial condition (1.5). Then, after solving for the Gaussian vortex centres, the vorticity is provided by (1.4). For any fixed $t > 0$ we aim at locating and categorising the critical points of the vorticity. These critical points will in general change with time, so we need to consider time as a bifurcation parameter in this approach. Notice that we use the notation Gaussian vortex centres for z_j, and extremal points of the vorticity for vortices. An important mathematical consequence of the symmetric initial condition turns out to be a closed-form expression for z_j implying a closed-form expression of the vorticity in the core-growth model which simplifies the characterisation of the critical points of the vorticity.

2. Numerical method

The core-growth model is compared with results from numerical solutions to the VTE, (1.1). The method used follows Dam *et al.* (2023), which we here briefly summarise alongside some specific details. The VTE is solved together with the Poisson equation for the streamfunction $\Delta\psi = -\omega$, giving the velocities $\partial_x\psi = -u_2$ and $\partial_y\psi = u_1$, where u_1 and u_2 are the velocity field vector components $\boldsymbol{u} = (u_1, u_2)$. We use a fourth-order Runge–Kutta integrator for the solution to the VTE, see E & Liu (1996*a*,*b*). The integrator time step is adaptive, and is implemented using extrapolation: at a given time t with

https://doi.org/10.1017/jfm.2026.11144 Published online by Cambridge University Press

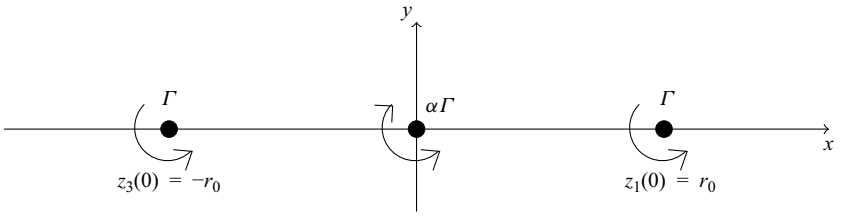


Figure 1. Initial conditions of the flow studied. Two equal point vortices are placed at $\pm(r_0, 0)$ with a centre point vortex with arbitrary strength and direction.

characteristic time step h, the next integrated value at time $h + t$ of the vorticity is found from both a single-step integration, denoted ω_h, and a two-step integration with time step $h/2$, denoted $\omega_{h/2}$. If $\max|\omega_h - \omega_{h/2}|/\max|\omega_h| > 0.01$ the time step is reduced by a factor 0.99 and it is otherwise increased by a factor 1.01. The spatial derivatives are approximated by the second-order central difference scheme, and the Poisson equation is solved using the spectral method, giving a significant speed up if the fast Fourier transform algorithm is applied.

The two-dimensional computational domain is set to $[-6; 6] \times [-6; 6]$ and discretised on a 512×512 grid. Periodic boundary conditions are applied in both directions. The initial time step is set to $h = 1 \times 10^{-6}$. We use $r_0 = 1$ and a vorticity strength of $\Gamma = 1$. Because the Dirac delta initial condition induces numerical instabilities, we initialise the integration from a slightly diffused system corresponding to time $\Delta x^2/4\nu$, where Δx is the grid spacing. Moreover, since we apply periodic boundary conditions the vorticity is shifted such that the total vorticity is zero. The effect of the domain size and initial time step size were tested in the case $\alpha = 1$ and $1 \leqslant Re \leqslant 1000$ by letting the domain be $[-12; 12] \times [-12; 12]$ (corresponding to a 1024×1024 grid) and $h = 2 \times 10^{-6}$. This showed no measurable difference on the computed merging time, which is found by tracking the vorticity extrema both visually and by numerical differentiation of the vorticity field. Finally, the Reynolds number is defined by $Re = \Gamma/\nu$, that is, the Reynolds number is controlled directly by the viscosity in (1.1).

3. Analysis of the core-growth model and comparison with the VTE

We proceed analysing the core-growth model with the initial conditions seen in figure 1. We first show that $z_1(t)$, $z_2(t)$ and $z_3(t)$ stay aligned by a fixation of z_2 and same angular velocities of z_1 and z_3.

The instantaneous velocity of the Gaussian vortex centres, z_j, given by (1.2) is perpendicular to the line through them, initially the x-axis as indicated in figure 1, suggesting that alignment of the Gaussian vortex centres is preserved. This is conveniently investigated by relying on the complex coordinate formulation. The ansatz of an aligned rotating configuration

$$z_k(t) = z_k(0)e^{i\phi(t)}\,, \quad k \in \{1, 2, 3\}\,, \quad \phi(0) = 0\,, \tag{3.1}$$

is inserted in (1.2) which is satisfied for

$$\frac{\mathrm{d}\phi(t)}{\mathrm{d}t} = \frac{\Gamma}{2\pi r_0^2}\left(\alpha\left(1 - e^{-\frac{r_0^2}{4\nu t}}\right) + \frac{1}{2}\left(1 - e^{-\frac{r_0^2}{\nu t}}\right)\right). \tag{3.2}$$

https://doi.org/10.1017/jfm.2026.11144 Published online by Cambridge University Press

As (3.2) is well defined for all $\nu t > 0$, the ansatz is verified and the initially aligned Gaussian vortices stay aligned, by fixation of the centre Gaussian vortex, with the two outer vortices rotating with identical angular velocity. For $\nu t \to 0$ the exponential terms vanish and the corresponding point vortex rotation rate is retrieved. For $\nu t \to \infty$, $\mathrm{d}\phi(t)/\mathrm{d}t \to 0$, i.e. the rotation rate vanishes due to viscosity.

Numerical computation of the rotation angle can be accomplished to machine precision using the exponential integral $Ei(x) = \int_x^\infty t^{-1} e^{-t} \mathrm{d}t$. To utilise this, (3.2) is integrated, relying on integration by parts and substitution to get

$$\phi(t) = \frac{\Gamma}{2\pi r_0^2}\left(\alpha\left(t - te^{-\frac{r_0^2}{4\nu t}} + \frac{r_0^2}{4\nu} Ei\left(\frac{r_0^2}{4\nu t}\right)\right) + \frac{1}{2}\left(t - te^{-\frac{r_0^2}{\nu t}} + \frac{r_0^2}{\nu} Ei\left(\frac{r_0^2}{\nu t}\right)\right)\right). \tag{3.3}$$

The positions of the Gaussian vortices are thus parametrised from (3.1) and (3.3).

For any fixed $t > 0$ we aim at describing the vorticity topology. This analysis is simplified by using a coordinate system with the x-axis along the Gaussian vortex centres, which is accomplished by a rotation of the original coordinate system by the angle $\phi(t)$. We define the viscous time, τ, position, vorticity, $\tilde{\omega}$, and $\tilde{z}$

$$\tau = \frac{4\nu}{r_0^2} t\,, \quad \tilde{\omega} = \frac{\pi r_0^2}{\Gamma}\omega\,, \quad \tilde{z} = \frac{1}{r_0} z. \tag{3.4}$$

Relabelling (dropping the tilde $\tilde{}$) the variables, the vorticity equation (1.4) appears as

$$\omega = \frac{1}{\tau}\left(\exp\left(-\frac{|z+1|^2}{\tau}\right) + \alpha \exp\left(-\frac{|z|^2}{\tau}\right) + \exp\left(-\frac{|z-1|^2}{\tau}\right)\right). \tag{3.5}$$

The Gaussian vortex centres, z_j, are fixed at $(0, 0)$ and $(\pm 1, 0)$ in the corotated system with the units introduced in (3.4). The task of investigating the vorticity topology is greatly simplified as the vorticity is explicitly parametrised depending on only two parameters, α and τ. Increasing ν corresponds to increasing τ i.e. by changing ν the same vorticity patterns will be observed, however, the transition timing changes. The parameter Γ does not affect the vorticity patterns – it acts as a scaling on the vorticity. Increasing Γ gives a linear scaling of the rotation rate given by (3.2) which in scaled variables becomes

$$\frac{\mathrm{d}\phi}{\mathrm{d}\tau} = \frac{\Gamma}{\nu}\frac{1}{8\pi}\left(\alpha\left(1 - e^{-\frac{1}{\tau}}\right) + \frac{1}{2}\left(1 - e^{-\frac{4}{\tau}}\right)\right). \tag{3.6}$$

To facilitate the further calculations we proceed using Cartesian coordinates where (3.5) is given by

$$\omega(x, y) = \frac{1}{\tau}\left(\exp\left(-\frac{(x+1)^2 + y^2}{\tau}\right) + \alpha \exp\left(-\frac{x^2 + y^2}{\tau}\right) + \exp\left(-\frac{(x-1)^2 + y^2}{\tau}\right)\right). \tag{3.7}$$

The vorticity field has reflection symmetry around the x and y axes, i.e. $\omega(-x, y) = \omega(x, y) = \omega(x, -y)$, and symmetry by rotation of π, i.e. $\omega(-x, -y) = \omega(x, y)$. The task is now to locate and characterise the critical points satisfying $\partial_x \omega(x, y) = \partial_y \omega(x, y) = 0$

$$\partial_x \omega = -\frac{2}{\tau^2}\exp\left(-\frac{x^2 + y^2}{\tau}\right)\left((x+1)\exp\left(-\frac{2x+1}{\tau}\right) + \alpha x + (x-1)\exp\left(\frac{2x-1}{\tau}\right)\right), \tag{3.8}$$

https://doi.org/10.1017/jfm.2026.11144 Published online by Cambridge University Press

$$\partial_y \omega = -\frac{2y}{\tau}\omega, \tag{3.9}$$

showing $(x, y) = (0, 0)$ is a critical point of the vorticity for any $\tau > 0$, and any α value. The higher-order derivatives needed to characterise the critical points are

$$\partial_{xx}\omega = -\frac{2x}{\tau}\partial_x\omega - \frac{2}{\tau^3}\exp\left(-\frac{x^2+y^2+1}{\tau}\right)\left((\tau - 2x - 2)\exp\left(-\frac{2x}{\tau}\right)\right.$$
$$\left. + \alpha\tau\exp\left(\frac{1}{\tau}\right) + (\tau + 2x - 2)\exp\left(\frac{2x}{\tau}\right)\right), \tag{3.10}$$

$$\partial_{yy}\omega = -\frac{2}{\tau}\omega - \frac{2y}{\tau}\partial_y\omega, \tag{3.11}$$

$$\partial_{xy}\omega = -\frac{2y}{\tau}\partial_x\omega. \tag{3.12}$$

At a critical point, $\partial_x\omega = \partial_y\omega = 0$, in particular $\partial_{xy}\omega = 0$ at any critical point.

3.1. *Three corotating vortices*

To proceed we distinguish between the cases $\alpha > 0$ and $\alpha < 0$, two symmetric vortices ($\alpha = 0$) having been studied elsewhere (Andersen *et al.* 2018). In this section we assume three corotating Gaussian vortices, $\alpha > 0$, which implies that the rotation rate (3.2), of the collinear Gaussian vortices is always positive i.e. the three Gaussian vortices rotate counter-clockwise at all times. The vorticity field, (3.7), is a sum of positive terms and therefore $y = 0$ is needed for $\partial_y\omega = 0$ by (3.9). To characterise a critical point, we have from (3.11), $\partial_{yy}\omega(x, 0) < 0$ and from (3.12), $\partial_{xy}\omega(x, 0) = 0$. Hence, if $\partial_{xx}\omega(x, 0) < 0$ at the critical point, then it is an extremum of the vorticity field i.e. a vortex. If $\partial_{xx}\omega(x, 0) > 0$ at the critical point, then it is a saddle. For $x \geqslant 1$, then $x + 1$, αx are positive and $x - 1$ is non-negative, so $\partial_x\omega < 0$ in this case i.e. there are no critical points for $x \geqslant 1$. The task of locating critical points of the vorticity is then reduced to finding zeros of $\partial_x\omega(x, 0)$ for $0 < x < 1$ for positive τ, α, where we may use that $\partial_x\omega$ is an odd function of x. Trivially, $(0, 0)$ is a critical point. For $\partial_{xx}\omega \neq 0$ at any critical point, the intersections of $\partial_x\omega(x, 0)$ with the x axis occur with non-zero slope of $\partial_x\omega$. Since $\partial_x\omega < 0$ for $x \geq 1$, the critical point with the largest x value has $\partial_{xx}\omega < 0$ and the sign of $\partial_{xx}\omega$ is alternating for decreasing x value. This implies that the outermost critical point of vorticity is a vortex, the next is a saddle, and so on with alternating type. The sign of $\partial_{xx}\omega(0, 0)$ carries important information; if it is positive, $(0, 0)$ is a saddle point of the vorticity and there are at least two more critical points which must be vorticity extrema

$$\partial_{xx}\omega(0, 0) = \frac{2}{\tau^2}\exp\left(\frac{1}{\tau}\right)\left(2\frac{2-\tau}{\tau}\exp\left(-\frac{1}{\tau}\right) - \alpha\right), \tag{3.13}$$

which for $\alpha > 0$ is negative for τ going to 0 or $\tau > 2$. Notice $2(2 - \tau)/\tau\exp(-1/\tau)$ is increasing for $\tau < 2/3$ and decreasing for $\tau > 2/3$ and has maximum value

$$\alpha_c = 4\exp\left(-\frac{3}{2}\right). \tag{3.14}$$

For $\tau_c = 2/3$ there are three scenarios, see figure 2: $0 < \alpha < \alpha_c$, $\alpha = \alpha_c$ and $\alpha > \alpha_c$. For $\alpha < \alpha_c$, $\partial_{xx}\omega(0, 0) < 0$ for small τ, increasing τ from a small value, $\partial_{xx}\omega(0, 0)$ changes sign for some $\tau < 2/3$ i.e. transforms from a vortex to a saddle, and for some $\tau > 2/3$, $\partial_{xx}\omega(0, 0)$ changes sign and $(0, 0)$ remains a vortex for all larger τ values. For $\alpha > \alpha_c$,

https://doi.org/10.1017/jfm.2026.11144 Published online by Cambridge University Press

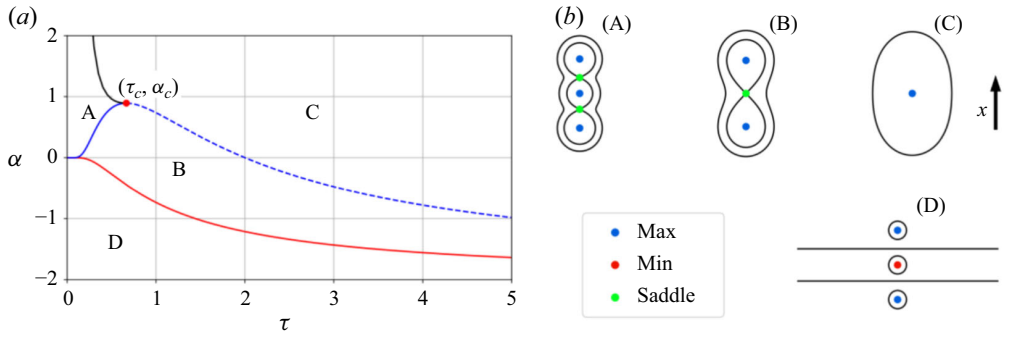


Figure 2. (*a*) Bifurcation diagram for the core-growth model. The four regions have distinct vorticity patterns. (*b*) Illustrations of the four vorticity patterns in the core-growth model.

$(0, 0)$ is a vortex for all positive τ. For the threshold case $\alpha = \alpha_c$, $(0, 0)$ is a vortex except for $\tau = 2/3$. A change in vorticity patterns occurs at a bifurcation point characterised by $\partial_x \omega(x, y) = \partial_{xx} \omega(x, y) = 0$. This implies from (3.13) that, in the parameter space (τ, α), the curve

$$\alpha = \left(\frac{4}{\tau} - 2\right) \exp\left(-\frac{1}{\tau}\right) \tag{3.15}$$

is a bifurcation curve (blue curve figure 2*a*). It is immediately clear that $\tau = 2$ is a solution to (3.15) for $\alpha = 0$, which was previously reported by Andersen *et al.* (2018) for the merging of two vortices.

The location of other bifurcation values can be computed from $\partial_x \omega(x, 0) = \partial_{xx} \omega(x, 0)$, which provides two equations for the three unknowns τ, α, x. From $\partial_x \omega(x, 0) = 0$, α can be solved for

$$\alpha = -\frac{x+1}{x} \exp\left(-\frac{2x+1}{\tau}\right) + \frac{1-x}{x} \exp\left(\frac{2x-1}{\tau}\right). \tag{3.16}$$

Inserting this expression into $\partial_{xx} \omega(x, 0) = 0$ gives one equation in the two unknowns x and τ. With the definition $s = 2x/\tau$ this equation can be solved for $x = f(s)$ with

$$f(s) = \coth(s) - \frac{1}{s}. \tag{3.17}$$

The procedure for locating bifurcation points is then: pick any $s > 0$, compute $x = f(s)$, $\tau = 2x/s$ and α from (3.16) provides a parametrisation of all bifurcation points, in particular adding the black curve in figure 2(*a*). This analysis results in a complete description of all emerging flow patterns and their transitions for $\alpha > 0$; see figures 2 and 3. For $\alpha > \alpha_c$, the initial vorticity field consisting of three aligned vortex maxima with a saddle between any two extrema (pattern (A)) merges to a single maxima and no saddles (pattern (C)) by two simultaneous saddle node bifurcations, where an outer vortex maximum and the nearest saddle merge and vanish (crossing the black curve in figure 2*a*), i.e. the centre vortex dominates. For $\alpha_c > \alpha > 0$ pattern (A) change to pattern (B) with increasing time as the middle vorticity extrema merge with the two neighbouring saddles through a pitchfork bifurcation (crossing the full blue curve in figure 2*a*) leaving a saddle at the origin, i.e. the centre vortex is suppressed. Then, pattern (B) changes to pattern (C) as an additional pitchfork bifurcation happens where the two outer vorticity maxima merge with the saddle (crossing the stipulated blue curve in figure 2*a*) and leave a single vorticity maxima at the origin (pattern (C)).

https://doi.org/10.1017/jfm.2026.11144 Published online by Cambridge University Press

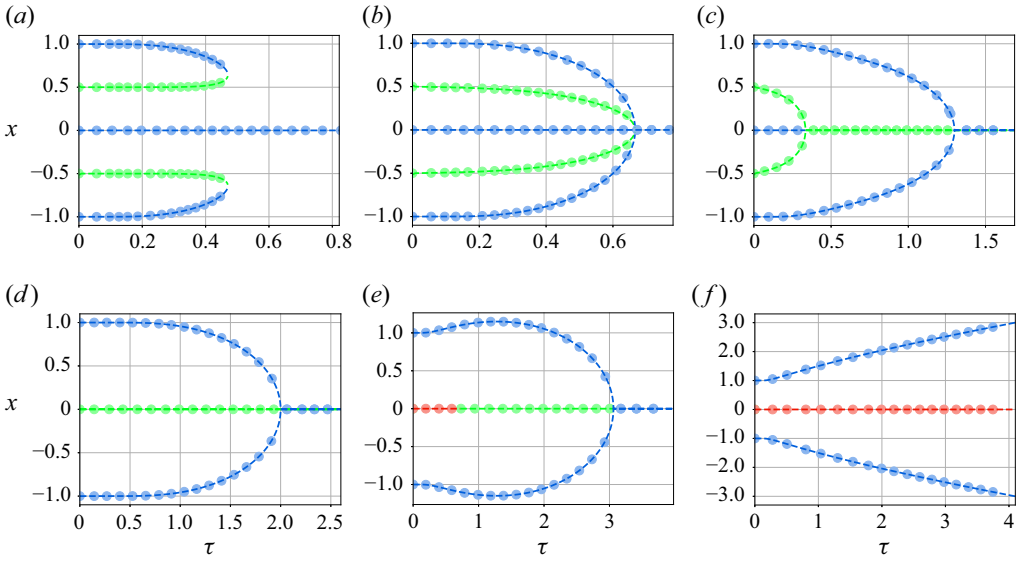


Figure 3. Position of critical points of the vorticity in the core-growth model (punctured curves) and for the VTE (dots) for $\Gamma/\nu = 1$ at different centre vortex strengths, α. Vorticity maxima (blue), vorticity minima (red) and vorticity saddles (green) are shown. Panel (*a*) for $\alpha = 1.0$, the vorticity pattern (A) persists until the outer vortices merge with the saddle points at $\tau = 0.48$, leading to vorticity pattern (C), i.e. the centre vortex dominates. Panel (*b*) for the threshold value $\alpha = \alpha_c$, vorticity pattern (A) persists until $\tau = 2/3$ where all critical points of vorticity collide in a double pitchfork bifurcation leaving a single vorticity maximum, pattern (C). Panel (*c*) for $\alpha = 0.5$, vorticity pattern (A) persists until $\tau = 0.35$, where a pitchfork bifurcation happens leading to vorticity pattern (B), i.e. centre vortex suppression, until a pitchfork bifurcation happens at $\tau = 1.3$ where vorticity pattern (C) persists after merging of the two outer vortices. Panel (*d*) for the threshold value $\alpha = 0$ (no centre Gaussian vortex), vorticity pattern (B) exists until merging at $\tau = 2$ where a pitchfork bifurcation leads to vorticity pattern (C), as previously described by Andersen *et al.* (2018). Panel (*e*) for $\alpha = -0.5$ the initial vorticity pattern is type (D), then turning into type (B) through an instant of a line of critical points of the vorticity (see (3.23)), i.e. the centre vortex is suppressed. Then vorticity pattern (B) turns into (C) by a pitchfork bifurcation, where the two outer extrema of vorticity collapse with the saddle of vorticity leaving a single vorticity extrema. Panel (*f*) for $\alpha = -2.5$, the vorticity pattern (D) persists as the outer vortices are moving outwards, i.e. the centre vortex dominates.

Trajectories of the critical points of vorticity can be obtained by numerically solving $\partial_x \omega(x, 0) = 0$ for fixed α. This is illustrated in the top row of figure 3 which compares very well with solutions of the VTE for $Re = 1$.

The intersection of the bifurcation curves that appears to be located at (τ_c, α_c) merits special attention. At this parameter set, $(x, y) = (0, 0)$ is a bifurcation point, which means a local investigation may be useful. We search for analytical expressions for critical points of the vorticity close to the origin by making a Taylor expansion of $(x + 1)\exp(-(2x + 1)/\tau) + \alpha x + (x - 1)\exp((2x - 1)/\tau)$, see (3.8), to sixth order in x with coefficients depending on τ and α. To accommodate for five critical points at least a fifth-order polynomial approximation, $p(x)$, of the vorticity is needed, which is given by

$$p(x) = x\left(\beta_1 + \beta_2 x^2 + \beta_3 x^4\right), \tag{3.18}$$

with coefficients

$$\beta_1 = \alpha - 2\frac{2 - \tau}{\tau}\exp\left(-\frac{1}{\tau}\right), \tag{3.19a}$$

https://doi.org/10.1017/jfm.2026.11144 Published online by Cambridge University Press

$$\beta_2 = \frac{4}{\tau^3}\exp\left(-\frac{1}{\tau}\right)\left(\tau - \frac{2}{3}\right), \tag{3.19b}$$

$$\beta_3 = \frac{4}{3\tau^5}\exp\left(-\frac{1}{\tau}\right)\left(\tau - \frac{2}{5}\right). \tag{3.19c}$$

The roots of the fifth-order polynomial, (3.18), can be analytically solved as only odd terms appear, one root is 0 and the remaining roots can be computed from the quadratic formula, solving for x^2. Notice that $\beta_1 = 0$ corresponds to the bifurcation curve (3.15). The roots of (3.18) are $x = 0$ and up to four more solutions

$$x = \pm\sqrt{\frac{-\beta_2 \pm \sqrt{D}}{2\beta_3}}, \tag{3.20}$$

with $D = \beta_2^2 - 4\beta_1\beta_3$. The curves in parameter space separating regions with one, three and five solutions are given by $\beta_1 = 0$ (figure 2 blue curve) and $D = 0$ (figure 2 black curve).

The root calculation of (3.18) is summarised as:

(i) for $\alpha < 2(2-\tau)/\tau\exp(-1/\tau)$ there are exactly three roots: $x = 0$, $x = \pm\sqrt{(-\beta_2 + \sqrt{D})/(2\beta_3)}$;
(ii) for $\alpha < 2(2-\tau)/\tau\exp(-1/\tau)$ and $\tau > 2/3$, $x = 0$ is the only root;
(iii) for $\alpha > \exp(-1/\tau)(15\tau^2 + 12\tau - 4)/(3\tau(-2+5\tau))$ and $\tau < 2/3$, $x = 0$ is the only root;
(iv) for $2(2-\tau)/\tau\exp(-1/\tau) < \alpha < \exp(-1/\tau)(15\tau^2 + 12\tau - 4)/(3\tau(-2+5\tau))$ and $\tau < 2/3$, there are five roots, $x = 0$ and $x = \pm\sqrt{(-\beta_2 + \sqrt{D})/(2\beta_3)}$.

The location and type of critical points analytically given by (3.20) are shown and compared with simulations of the VTE in figure 4, showing good agreement for critical points of vorticity close to 0, as expected, which is ensured by letting α being close to α_c. The roots of p and the explicit parametrisation with τ as a bifurcation parameter provides a low-order form of the bifurcations near (τ_c, α_c) with a double pitchfork bifurcation at this point.

The observed vorticity patterns in the core-growth model accurately predict the vorticity patterns for low Re of the VTE. On increasing Re, the qualitative description remains correct. However, the bifurcation curves in (τ, α) shift to the left and α_c moves upwards for $Re = 50$ and $Re = 100$, see figure 5.

Increasing Re further, new vorticity patterns emerge for $Re > 1290$, see figure 6. The additional vortex structures emerge as two simultaneous saddle node bifurcations occur in the shear layer far from the existing vortices, giving pattern B^1. Then, a pitchfork bifurcation happens close to the origin, resulting in pattern C^1 before the outer vortices disappear again simultaneously through saddle node bifurcations, resulting in a single vorticity extremum, pattern C.

3.2. *Counter-rotating centre vortex*

We now proceed by analysing the case $\alpha < 0$, i.e. the centre Gaussian vortex rotates in the opposite direction to the two outer Gaussian vortices. The rotation rate of the three Gaussian vortex centres, (3.6), now consists of two terms with opposite sign. For $\alpha > -0.5$ the configuration is always rotating counter-clockwise, for $\alpha < -2$ the configuration

https://doi.org/10.1017/jfm.2026.11144 Published online by Cambridge University Press

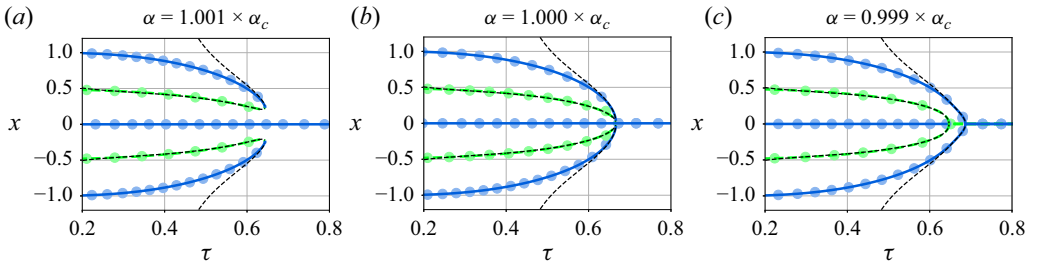


Figure 4. Full blue and green curves are critical points of vorticity from the core-growth model, dots are based on the VTE ($Re = 1$). Blue are maxima and green are saddles. The Taylor approximation of the position of critical points in the core-growth model ((3.18)) is shown with black stipulated curves. For positions of the critical points of the vorticity close to $x = 0$, the Taylor approximation is approximating the VTE well.

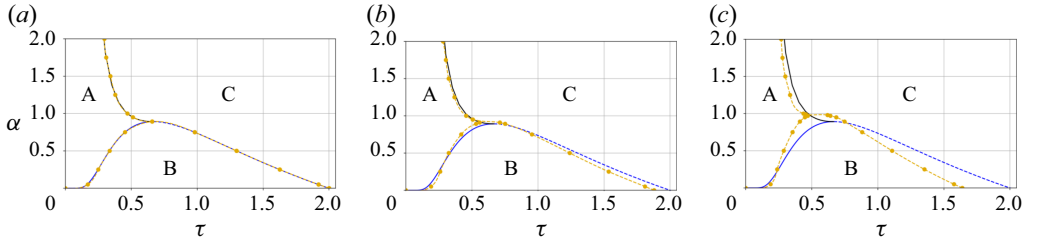


Figure 5. Comparison between the vorticity patterns from the core-growth model and VTE simulations at $Re = 1$ (a), $Re = 50$ (b) and $Re = 100$ (c). Blue curve is the core-growth model, yellow are VTE simulations. The threshold between centre vortex dominance ($A \to C$) and suppression ($A \to B \to C$) is increased from $\alpha = 0.9$ to $\alpha = 1.0$ on increasing Re from 1 to 100.

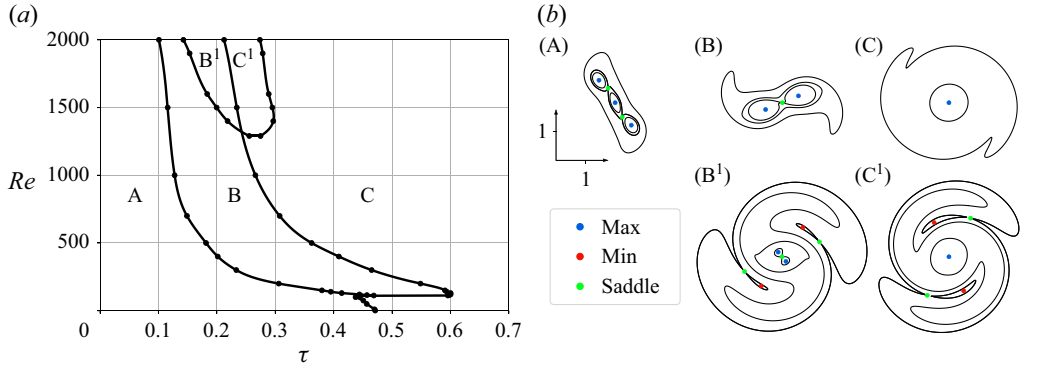


Figure 6. (a) Bifurcation diagram for varying Re at $\alpha = 1$ based on the VTE. For $Re > 1290$ there is a time interval with two extra pairs of saddle minimum points around the original topology compared with the core-growth model, B^1 and C^1. (b) Examples of the five different topologies ($Re = 1600$).

always rotates clockwise and for $-2 < \alpha < -0.5$ the configuration first rotates clockwise and then changes direction to rotate counter-clockwise. This phenomenon is also observed in numerical solutions of VTE, see figure 7.

In the core-growth model, the point $(x, y) = (0, 0)$ is yet again a critical point of vorticity so that (3.15) is a bifurcation curve for negative α and for $\tau > 2$, see figure 2(a). Likewise, $\partial_x \omega(x, 0) = \partial_{xx} \omega(x, 0) = 0$ will provide a bifurcation point implying that (3.16) and (3.17) can be used to compute these points for various α and τ. However, in contrast

https://doi.org/10.1017/jfm.2026.11144 Published online by Cambridge University Press

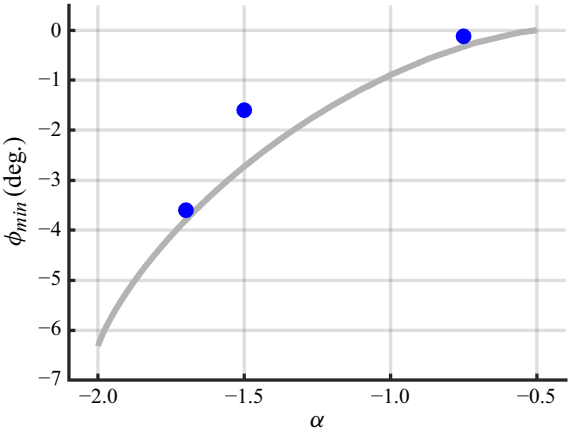


Figure 7. The configuration of three Gaussian vortices changes direction from clockwise to counter-clockwise for $-2 < \alpha < -0.5$. The minimal angle decreases as α approaches -2. Grey curve is the core-growth model (analytically solving $\mathrm{d}\phi/\mathrm{d}t = 0$), blue dots are VTE for $Re = 1$.

to a corotating centre vortex, critical points of vorticity off the x-axis are also possible as $\partial_y \omega = 0$ can be obtained for $\omega = 0$, see (3.9). From (3.7), this criterion is equivalent to

$$\exp\left(\frac{2x}{\tau}\right) + \exp\left(-\frac{2x}{\tau}\right) + \alpha \exp\left(\frac{1}{\tau}\right) = 0, \tag{3.21}$$

which is independent of y and symmetric in x. The equation is equivalent to a second-order polynomial in $\exp(2x/\tau)$ which can be solved to

$$x_+ = \frac{\tau}{2} \ln\left(\frac{-\alpha \exp\left(\frac{1}{\tau}\right) + \sqrt{\alpha^2 \exp\left(\frac{2}{\tau}\right) - 4}}{2}\right), \tag{3.22}$$

with the other root being $x_- = -x_+$. Hence, when $\omega = 0$ is solvable, there are horizontal level curves of zero vorticity symmetrically located on the x-axis. These two level curves collapse when the discriminant is zero

$$\alpha = -2 \exp\left(-\frac{1}{\tau}\right), \tag{3.23}$$

which is the red curve on figures 2 and 8. Comparing with the blue bifurcation curve given by (3.15) we see that the blue curve always lies above the red curve, and that both curves approach -2 as $\tau \to \infty$. Considering figure 2 this means that for $\tau \to \infty$ the region C expands and approaches the lower bound $\alpha = -2$ from above and the region D shrinks with upper bound $\alpha = -2$ with region B being squeezed in between regions C and D. For parameter values satisfying (3.23), $x = 0$ is the single solution to $\omega(x, y) = 0$, implying that the y-axis satisfies $\partial_y \omega(x, y) = 0$. As $\partial_x \omega(0, y) = 0$ (see (3.8)) this means that the y-axis is a continuum of critical points when (3.23) is satisfied.

The right-hand side of (3.23) is a decreasing function of τ with values between 0 and 2. Hence, for fixed $0 > \alpha > -2$ there is a unique τ such that (3.23) is satisfied. Crossing the curve given by (3.23) implies a sign change in $\partial_{yy}\omega(0, 0)$, which changes $(0, 0)$ from a minimum to a saddle point of the vorticity, see figures 3(*e*) and 9. This implies that the centre vortex is suppressed. For $\alpha < -2$ the discriminant of (3.22) is always positive,

https://doi.org/10.1017/jfm.2026.11144 Published online by Cambridge University Press

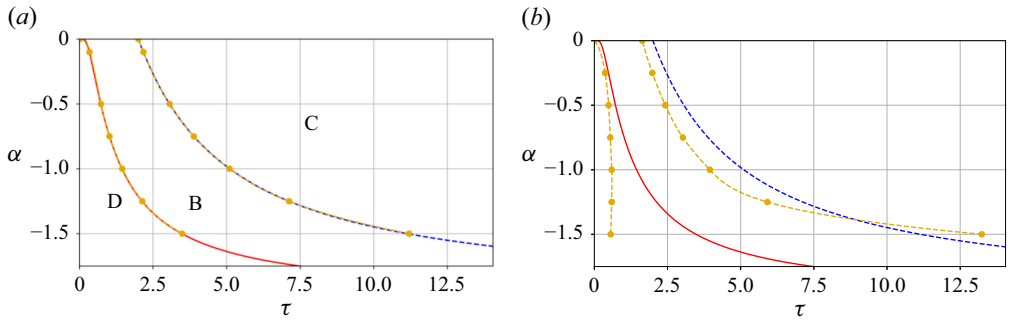


Figure 8. Bifurcation diagram for counter-rotating centre vortex at (*a*) $Re = 1$ and (*b*) $Re = 100$. Red and blue curves are the core-growth model, yellow curves are simulations of VTE. For increasing Re the transition $D \to B \to C$ (centre vortex dominates) happens faster.

so the vertical vorticity contours never collapse, implying that $(0, 0)$ remains a vorticity minimum, see figures 3(*f*) and 2.

Hence, for $\alpha < 0$ there are two distinct vorticity regimes, for $-2 < \alpha < 0$, first the centre vortex is suppressed by turning a vorticity minimum into a saddle point, then the outer vortex maxima will eventually collide with the saddle point at $(0, 0)$ and from then on, a unique vorticity maximum located at $(0, 0)$ persists, see figure 3(*e*). For $\alpha < -2$, $(0, 0)$ remains a minimum, and the maxima are pushed to infinity i.e. the centre vortex dominates, see figure 3(*f*). The core-growth model is compared with the VTE in figure 8, showing good quantitative and qualitative agreement for decreasing Re.

3.2.1. *Asymptotic behaviour*

For $\alpha \to -2^+$ an interesting similarity of the vorticity patterns is observed, see figure 9. The first bifurcation, where the vorticity minimum at the origin becomes a saddle, appears to happen at a third of the time to the second bifurcation of the origin, where the two outer branches merge, leaving a vorticity maximum at the origin. The first bifurcation is given by (3.23) and the second by (3.15). For large τ these expressions can be approximately inverted by letting $k = 1/\tau$ and linearising the expressions for $k = 0$ to first order to obtain the following approximation to (3.23):

$$\tau_1 = \frac{2}{\alpha + 2}, \tag{3.24}$$

and the approximate solution of (3.15)

$$\tau_2 = \frac{6}{\alpha + 2}, \tag{3.25}$$

showing that the second bifurcation happens a factor three later than the first bifurcation ($\tau_2 = 3\tau_1$). To characterise the similarity in shape of the outer critical points of vorticity, the largest value of these critical points is calculated. To obtain this, we will assume the x value is large, hence x^{-1} is small (a symmetric solution is located at $-x$). Then $x = x(\tau_3)$ is implicitly defined by $\partial_x \omega(x, 0) = 0$. Calculating $x'(\tau_3) = 0$ by use of (3.8) allows for calculating $\tau_3(x)$ at the largest x-value. Inserting this relation in $\partial_x \omega(x, 0) = 0$, letting $K = 1/x$, Taylor expanding in K and substituting back to τ_1 we obtain

$$\tau_3 = \frac{3}{\alpha + 2}, \tag{3.26}$$

https://doi.org/10.1017/jfm.2026.11144 Published online by Cambridge University Press

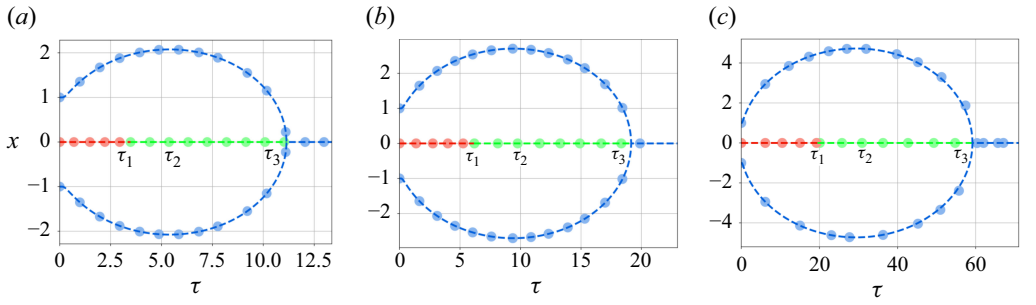


Figure 9. Positions of critical points of the vorticity in the core-growth model for $\alpha = -1.5$ (a), -1.7 (b) and -1.9 (c). Blue curve shows maxima, red curves show minima, green curves show saddles. Dots are VTE simulations at $Re = 1$. The vorticity patterns change from (D) to (B) to (C), see figure 2.

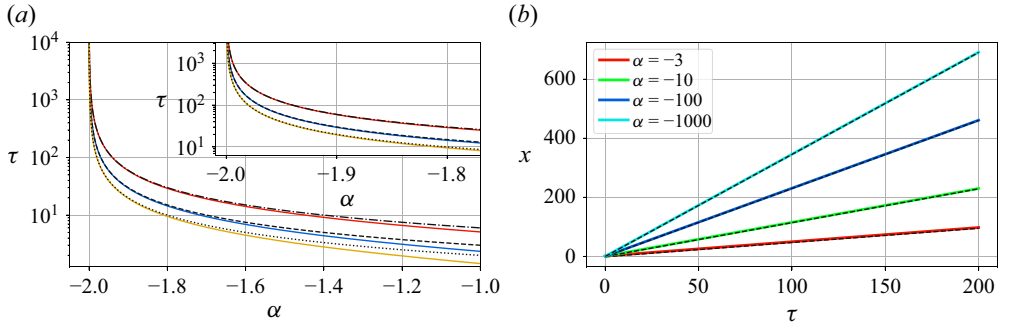


Figure 10. (a) Explicit asymptotic expressions for τ close to -2, τ_1 (yellow), τ_2 (red), τ_3 (blue), given by (3.24), (3.25), (3.26) compared with numerical solutions of the core-growth model (black). (b) Position of vorticity maxima of the core-growth model compared with explicit asymptotic expressions (dashed), valid for large x, (3.27). A symmetric branch of extrema is located at $-x$.

showing that the maximal x value for a critical point is happening at half the time of the collapse of the two outer branches ($\tau_3 = 0.5\tau_2$). Hence, for $\alpha \to -2^+$, the characteristic times τ_1, τ_2, τ_3 scale similarly, which can be observed in figures 9 and 10.

For $\alpha < -2$ approximate trajectories of the vorticity maxima may be derived. Anticipating a solution to $\partial_x \omega(x, 0) = 0$ for a large x which occurs for $\alpha < -2$, it is a good approximation to assume $x - 1 \approx x \approx x + 1$, in which case the solutions to $\partial_x \omega(x, 0) = 0$ are identical to the solutions of $\omega(x, 0) = 0$ i.e. $\partial_x \omega(x, 0) = 0$ is solved by (3.22). As τ will also be large, $\exp(1/\tau) \approx 1$ we have for $\alpha < -2$ that $\partial_x \omega(x, 0) = 0$ is approximately solved by

$$x = \frac{1}{2} \ln \left(\frac{|\alpha|}{2} + \frac{1}{2} \sqrt{|\alpha|^2 - 4} \right) \tau. \tag{3.27}$$

Hence, for $\alpha < -2$ and large x, the position of the outer vorticity maxima increases linearly with τ and a slope increasing with $|\alpha|$, see figures 3(f) and 10.

4. Discussion

We investigate the evolving vorticity topology to characterise the vortex dynamics of a flow initiated by three aligned vortices for any strength of the centre vortex and two identical outer vortices. The core-growth model allows for a complete investigation

https://doi.org/10.1017/jfm.2026.11144 Published online by Cambridge University Press

and detailed analytical characterisation and is a useful approximation to the VTE for low *Re*. Four qualitatively distinct vorticity patterns are observed separated in parameter space by $\alpha = \alpha_c = 4\exp(-3/2)$, $\alpha = 0$ and $\alpha = -2$, the latter corresponding to the limiting case where the sum of the inner vortex and the two outer vortices vanishes, see figure 2. For α-values near α_c, three different vorticity patterns are present. We derive explicit, simple formulas for α near α_c for location and type of the critical points of vorticity, as the roots of a polynomial ((3.18) and figure 4), which is a new contribution to normal forms of bifurcations subject to symmetry. The degenerate case $\alpha = \alpha_c$ corresponds to two pitchfork bifurcations happening simultaneously. Brøns (2007) provides a catalogue of other cases investigated in terms of the streamline topology.

For $-2 < \alpha < -0.5$ the three Gaussian vortices first rotate clockwise and then change direction of rotation, still maintaining a relative equilibrium. This exotic behaviour is also found when comparing with the VTE. Such dynamics cannot be found in the point vortex model of any configuration and is the first of its kind reported for Gaussian vortices. Jing *et al.* (2010) find that a three vortex configuration starts to rotate in the core-growth model but not in the point vortex model, i.e. the rotation is viscously induced. They studied a unique value of α, for other fixed α values we observe a shift of direction of rotation. As $\alpha \to -2^+$ the two vorticity extrema first separate but eventually merge (figure 10). We derive expressions for both cases, and find a scaling relationship for qualitative flow features ((3.24), (3.25) and (3.26)). If $\alpha < -2$ the two vorticity extrema are pushed to infinity with increasing time, see (3.27).

The vorticity patterns are qualitatively and quantitatively similar for the core-growth model and VTE for low *Re;* see figures 3, 5, 8 and 9. Simple expressions of the trajectories of the vorticity extrema are derived. For the case of three equal vortices, increasing *Re* beyond 1290 implies new vortices are generated in an outer shear layer which is not captured by the core-growth model, see figure 6.

For $\alpha < 0$ the vorticity pattern in the core growth is dependent on the collapse of two horizontal null clines, $\partial_y \omega(x, y) = 0$ creating a transitory line of critical points. This phenomenon is structurally unstable, i.e. a small perturbation to the equations will lead to a different scenario. As the core-growth model is only an approximation to the true viscous behaviour of the VTE, one may expect that the approximation is less favourable for $\alpha < 0$ than has been observed for $\alpha \geqslant 0$. Figure 8 shows good quantitative agreement for $Re = 1$ and some qualitative agreement for $Re = 100$. However, owing to the structurally unstable core-growth model for $\alpha < 0$, an additional transition in the vorticity pattern is observed for $Re = 100$, see figure 11. The two horizontal null clines of $\partial_y \omega(x, y) = 0$ in the core-growth model bend towards each other in the VTE simulation, creating a pitchfork bifurcation at (0, 0), generating the transition from pattern (D) to pattern (B^2). Then the newly generated vorticity minima are pushed outwards, and a bifurcation happens, where a heteroclinic vorticity level curve encapsulates all vortex minima and maxima in a four-leaf clover vorticity pattern (panel B^{2-3}). After this the two vortex maxima are joined by a heteroclinic level curve – as described by the core-growth model, while the two vortex minima move outwards and away. The vortex maxima and saddle point then merge as expected from the core-growth model.

In general, a richer dynamics can be observed in three-dimensional flow than in two-dimensional flow. For example, the occurrence of hairpin vortices, which can be described based on bifurcation analysis and the so-called Q-criterion (Ozdemir & Brøns 2025). It is beyond the scope of the present paper to address a full analysis of three-dimensional vortex merging of three aligned vortices.

In conclusion, the two-dimensional vortex merging of three aligned vortices is investigated and classified relying on critical points of the vorticity. The core-growth

https://doi.org/10.1017/jfm.2026.11144 Published online by Cambridge University Press

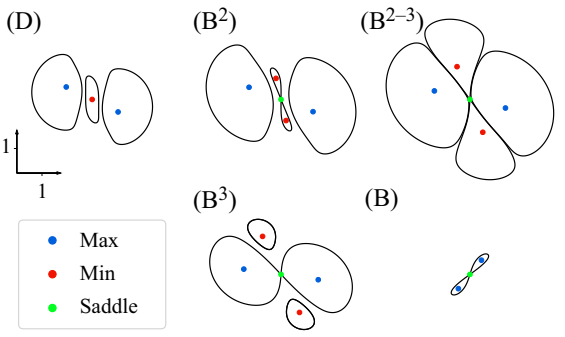


Figure 11. Vorticity patterns at $\alpha = -1$ and $Re = 100$ for simulations of the VTE. (D) Same topology as in the core-growth model (see figure 2D). (B^2) A pitchfork bifurcation implies a minimum is transformed into a saddle and two minima. (B^{2-3}) The transition between topology (B^2) and (B^3) where the saddle point contour is a heteroclinic connection around each minimum and maximum – the 'four-leaf clover' pattern. (B^3) The vorticity contour through the saddle-point encloses the two maxima, and the minima move away. (B) Same pattern as in the core-growth model (see figure 2B) before merging to a single maxima.

model provides a useful approximation for the vorticity patterns and transitions for low Re and enables analytical investigations.

Declaration of interests. The authors report no conflict of interest.

References

Andersen, M., Schreck, C., Hansen, J.S. & Brøns, M. 2018 Vorticity topology of vortex pair interactions at low Reynolds numbers. *Eur. J. Mech. B – Fluids* **74**, 58–67.

Aref, H. 1979 Motion of three vortices. *Phys. Fluids* **22** (3), 393–400.

Brøns, M., Ozdemir, I.R., Heil, M., Andersen, M. & Hansen, J.S. 2025 Dynamics and bifurcations of critical points of vorticity, with application to vortex merging. *J. Fluid Mech.* **1010**, A64.

Brøns, M. 2007 Streamline topology: patterns in fluid flows and their bifurcations. In *Advances in Applied Mechanics*, vol. 41, pp. 1–42. Elsevier.

Cerretelli, C. & Williamson, H.K. 2003 The physical mechanism for vortex merging. *J. Fluid Mech.* **475**, 41–77.

Dam, M.J.B., Hansen, J.S. & Andersen, M. 2023 Viscous merging of three vortices. *Eur. J. Mech. B – Fluids* **99**, 17–22.

E, W. & Liu, J.G. 1996*a* Finite difference schemes for incompressible flows in vorticity formulations. *ESAIM: Proc.* **1**, 181–195.

E, W. & Liu, J.G. 1996*b* Vorticity boundary conditions and related issues for finite difference schemes. *J. Comput. Phys.* **124**, 368–382.

Gallay, T. & Wayne, C.E. 2005 Global stability of vortex solutions of the two-dimensional Navier–Stokes equation. *Commun. Math. Phys.* **255** (1), 97–129.

van Heijst, G.J.F. & Kloosterziel, R.C. 1989 Tripolar vortices in a rotating fluid. *Nature* **338** (6216), 569–571.

Heil, M., Rosso, J., Hazel, A.L. & Brøns, M. 2017 Topological fluid mechanics of the formation of the Kármán-vortex street. *J. Fluid Mech.* **812**, 199–221.

Jing, F., Kanso, E. & Newton, P.K. 2010 Viscous evolution of point vortex equilibria: the collinear state. *Phys. Fluids* **22** (12), 123102.

Jing, F., Kanso, E. & Newton, P.K. 2012 Insights into symmetric and asymmetric vortex mergers using the core growth model. *Phys. Fluids* **24**, 073101.

Kim, S. & Sohn, S. 2012 Interactions of three viscous point vortices. *J. Phys. A: Math. Theor.* **45** (45), 455501.

Leweke, T., Dizes, S.L. & Williamson, C.H.K. 2016 Dynamics and instabilities of vortex pairs. *Annu. Rev. Fluid Mech.* **48** (1), 507–541.

Meunier, P., Le Dizes, S. & Leweke, T. 2005 Physics of vortex merging. *C. R. Phys.* **2005**, 431–450.

Nielsen, A.R., Andersen, M., Hansen, J.S. & Brøns, M. 2021 Topological bifurcations of vortex pair interactions. *J. Fluid Mech.* **917** (917), 23.

https://doi.org/10.1017/jfm.2026.11144 Published online by Cambridge University Press

OZDEMIR, I.R. & BRØNS, M. 2025 Bifurcations of Q-vortices. *Phys. Fluids* **37** (4), 044113.
SYNGE, J.L. 1949 On the motion of three vortices. *Can. J. Maths* **1** (3), 257–270.
TOBAK, M. & PEAKE, D.J. 1982 Topology of three-dimensional separated flows. *Annu. Rev. Fluid Mech.* **14** (1), 61–85.
WIDNALL, S.E. 1975 The structure and dynamics of vortex filaments. *Annu. Rev. Fluid Mech.* **7**, 141–165.

https://doi.org/10.1017/jfm.2026.11144 Published online by Cambridge University Press